Intermetallics 18 (2010) 954–960

Contents lists available at ScienceDirect

Intermetallics

journal homepage: www.elsevier.com/locate/intermet

Structural relaxation and self-repair behavior in nano-scaled Zr–Cu metallic glass under cyclic loading: Molecular dynamics simulations

Y.C. Lo [a], H.S. Chou [a], Y.T. Cheng [a], J.C. Huang [a,*], J.R. Morris [b,c], P.K. Liaw [b]

[a] Department of Materials and Optoelectronic Science; Center for Nanoscience and Nanotechnology, National Sun Yat-Sen University, Kaohsiung 804, Taiwan, ROC
[b] Department of Materials Science and Engineering, The University of Tennessee, Knoxville, TN 37996-2200, USA
[c] Materials Science and Technology Division, Oak Ridge National Laboratory, P.O. Box 2008, Oak Ridge, TN 37831-6115, USA

ARTICLE INFO

Article history:
Received 12 October 2009
Received in revised form
27 December 2009
Accepted 14 January 2010
Available online 16 February 2010

Keywords:
E. Simulations, atomistic
B. Glasses, metallic
B. Fatigue resistance and crack growth
B. Plastic deformation mechanisms

ABSTRACT

Bulk metallic glasses are generally regarded as highly brittle materials at room temperature, with deformation localized within a few principal shear bands. In this simulation work, it is demonstrated that when the Zr–Cu metallic glass is in a small size-scale, it can deform under cyclic loading in a semi-homogeneous manner without the occurrence of pronounced mature shear bands. Instead, the plastic deformation in simulated samples proceeds via the network-like shear-transition zones (STZs) by the reversible and irreversible structure-relaxations during cyclic loading. Dynamic recovery and reversible/irreversible structure rearrangements occur in the current model, along with annihilation/creation of excessive free volumes. This behavior would in-turn retard the damage growth of metallic glass. Current studies can help to understand the structural relaxation mechanism in metallic glass under loading. The results also imply that the brittle bulk metallic glasses can become ductile with the sample size being reduced. The application of metallic glasses in the form of thin film or nano pieces in micro-electro-mechanical systems (MEMS) could be promising.

1. Introduction

The metallic glasses (MGs) are potential metallic materials due to their interesting properties, such as the high strength, high elastic strain limit, and high wear/corrosion resistance [1–3]. However, the insufficient plastic deformation is the drawback for applications. Tremendous efforts have been made to improve the mechanical properties of BMGs under monotonic or cyclic loading. The concept of free volume is viewed as the main defects in the metallic glasses, because free volumes can offer the requisite special sites for the atomic shear movement to deform in the glass. The movement of free volumes results in the formation of the shear-transition zone (STZ), which is believed to be the basic flow defect contributing local strain in the metallic glass upon loading [4–6]. Plastic deformation of metallic glasses contains homogeneous and inhomogeneous flow usually, depending on the temperature, applied stress/strain level, and glass condition.

Inhomogeneous flow in metallic glasses results from high stress concentration at lower temperatures and causes the shear localization processes as well as formation of shear bands. Many studies have investigated the relationship between the free volume and the formation of shear bands [7–9]. Atomic simulations also show that the local free volumes increase in the BMGs provides an open space for the movements of atoms and is associated with the localization of shear band, and the shear softening results from the production of excessive free volume in the shear band [10–12]. In the fatigue damage of BMGs, the shear band formation and propagation usually go along with the local increase of free volumes and crack sites within BMGs due to the weakness in the shear bands or shear-off steps [13,14], subsequently leading a fracture and fatigue damage. In contrast, the homogenous shear flow in metallic glass typically occurs within the supercooled liquid region at high temperatures near the T_g point and provides well plastic deformation properties. However, atomic simulations indicated that the shear localization of MGs not only depends on its thermal history but also on the length-scale of sample [10,15,16].

Lately, experimental studies show a sample-size effect on the BMG mechanical properties. Under a certain small size-scale, the development of shear band becomes homogeneous deformation when the metallic glasses are subjected to tension or compression loading at room temperature [17–19]. The plasticity of MGs

* Corresponding author. Tel.: +886 7 5252000x4063; fax: +886 7 5254099.
E-mail address: jacobc@mail.nsysu.edu.tw (J.C. Huang).

0966-9795/$ – see front matter © 2010 Elsevier Ltd. All rights reserved.
doi:10.1016/j.intermet.2010.01.012

between inhomogeneous and homogeneous flows is also related to their packing density states [20,21]. It is worthy to study cyclic deformation of MGs under homogeneous mechanical response. The aim of this paper is to examine the relationship between the variation of free volume and the basic development of shear deformation events under cyclic loading in small size-scale, and to further understand the mechanism of deformation under cyclic-loading process in homogeneous flows.

2. Simulation details

The current simulation model consisted of 47,424 atoms, in a mixture of 50% (atomic percent) Zr and 50% Cu in a box size of 9.5 nm × 9.5 nm × 9.5 nm, as shown in Fig. 1(a). This composition of Zr–Cu binary alloy has good glass forming ability [22] and the lowest packing density for homogeneous flow [21]. Atomic interactions between each particle were described by the many-body and tight-binding potential using the following equation [23,24]:

$$E_i = -\left\{\sum_j \xi^2 \exp\left[-2q\left(\frac{d_{ij}}{d_0}-1\right)\right]\right\}^{1/2} + \sum_j A\exp\left[-p\left(\frac{d_{ij}}{d_0}-1\right)\right], \quad (1)$$

where ξ is an effective hopping integral, d_{ij} is the distance between atoms, i and j, and d_o is the first-neighbor distance. The parameters, A, p, and q, are determined by the experimentally obtained values of the cohesive energy, lattice parameter, bulk modulus, and shear elastic constants. The parameters of the tight-binding potential for Zr and Cu employed in the current simulation were proposed by Duan *et al.* [24]. The potentials have been shown to be in good agreement with the experiments. The Nose-Hoover chain method [25,26] was used to control the temperature and pressure to obtain the reasonable thermodynamic state in the whole MD-simulation process as well as to bring the imposed tension loading on the simulation model. The equations of motion for the positions and momenta that generate the isobaric–isothermal ensemble in Nose-Hoover chain method are [25,26]:

$$\dot{\gamma}_i = \frac{P_i}{m_i} + \frac{p_\varepsilon}{W}\gamma_i, \quad (2)$$

$$\dot{P} = F_i - \left(1+\frac{d}{N_f}\right)\frac{p_\varepsilon}{W}P_i - \frac{p_\xi}{Q}P_i, \quad (3)$$

where N_f is the degree of freedom for the number of particles in d dimensions. The symbols ξ, p_ξ, and Q are the coordinate, momentum and effective mass which are used to describe the thermostate in the Nosé-Hoover chain. The symbols, ε, p_ε and W, are the barostat variables similar to the version of thermostat.

$$\dot{V} = \frac{\mathrm{d}Vp_\varepsilon}{W}, \quad (4)$$

$$\dot{p}_\varepsilon = \mathrm{d}V(p_{\mathrm{int}} - p_{\mathrm{ext}}) + \frac{d}{N_f}\sum_{i=1}^{N}\frac{P_i^2}{m_i} - \frac{p_\xi}{Q}p_\varepsilon, \quad (5)$$

$$\dot{\xi} = \frac{p_\varepsilon}{Q}, \quad (6)$$

$$\dot{p}_\xi = \sum_{i=1}^{N}\frac{P_i^2}{m_i} + \frac{P_\varepsilon^2}{W} - \left(N_f+1\right)kT, \quad (7)$$

In the equation, p_{ext} is the external pressure or imposed stress, and p_{int} is internal pressure, which can be calculated during the simulation process from virial equation,

$$p_{\mathrm{int}} = \frac{1}{\mathrm{d}V}\left[\sum_{i=1}^{N}\frac{P_i^2}{m_i} + \sum_{i=1}^{N}\gamma_i\cdot F_i - (\mathrm{d}V)\frac{\partial\phi(\gamma,V)}{\partial V}\right]. \quad (8)$$

The values of frequencies for effective mass are chosen in 0.0004 for thermostate and 0.0001 for barostate for optimum converging toward the equilibrium states. Periodic boundary conditions were employed in all three dimensions. The glassy structure was obtained by quenching the sample model at a cooling rate 5 K/ps (ps = 10^{-12} s) from 2000 down to 300 K, followed by an equilibrium for 30,000 time steps. The glass transition was found to be about 650 K according to the volume versus temperature diagram. The average density is about 7.29 g/cm^3, and the potential energy at this as-quenched state is about −5.233 eV. Because the difference of densities between the samples cooled at 1 and 10 K/ps is 0.096%, the density is considered insensitive to the cooling rate of the Zr–Cu BMG [12].

The stress-control modes are applied in this simulation. The uniaxial stress-control mode was first applied along the Z axis to

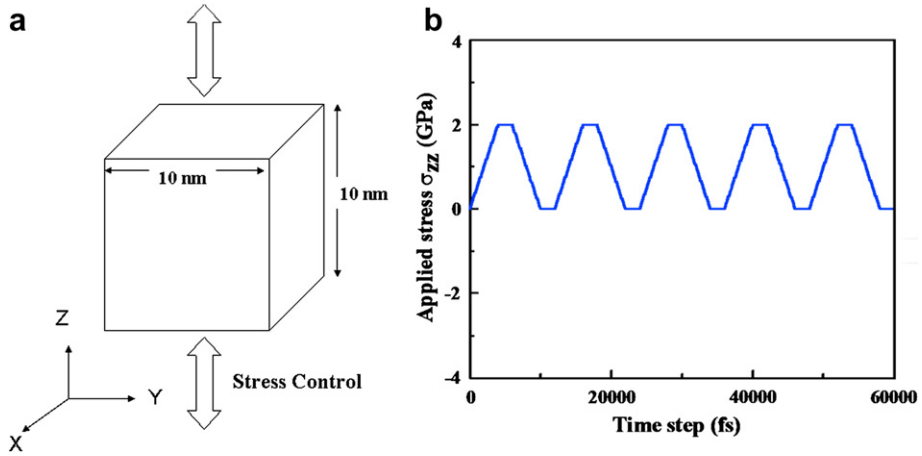

Fig. 1. Cyclic-loading conditions during MD-simulations of Zr–Cu metallic glass: (a) schematic illustration of the geometry used in the stress-control mode (the arrows indicate the direction of applied loading), and (b) the stress-control mode for a tension fatigue experiment at $\sigma_{\max} = 2$ GPa.

implement the tension cyclic-loading tests. To induce the initiation of deformation in the simulation model during the cyclic-loading process, the maximum tensile stress amplitude, σ_{max}, was chosen to be 2 GPa, and the induced-strain level during each loading cycle was around 2.8%. Note that the 2 GPa stress amplitude might appear to be too high judging from the fact that the fracture tensile or compression stress for bulk Zr–Cu amorphous specimen may only be around 1.5–1.8 GPa. But because of the size effect [27,28], the stress level in micro- or nano-scale can increase to more than 2.5–3 GPa. The minimum stress, σ_{min}, was set to zero, equivalent to complete unloading; the stress ratio $\sigma_{min}/\sigma_{max}$ is equal to zero. The applied load was increased gradually at a rate of 0.5 MPa/fs (fs $= 10^{-15}$ s) until the maximum tensile stress and then was held for 2000 fs to reach a relatively equilibrium state, and vice versa. The tensile fatigue cycle is set to be 100 and stress in both x and y directions is maintained at zero during the whole processes. The period of one cycle is 12,000 fs. The applied cycling load is presented in Fig. 1(b).

3. Microscopic deformation of cyclic loading

To observe the deformation events at the atomic scale, we present the ABRA method [11] to demonstrate where the local shear strains appear under cyclic loading. The ABRA is quantified by calculating the change of angle φ_{ij} between mutual orientations of the nearest-neighbor bond vectors. The angle φ_{ij} is given by

$$\varphi_{ij} = \cos^{-1}\left(\frac{\gamma_{ij}\cdot\gamma'_{ij}}{\left|\gamma_{ij}\right|\left|\gamma'_{ij}\right|}\right), \tag{9}$$

where $r_{ij}$and $\gamma'_{ij}$are the nearest-neighbor bond vectors before and after deformation. While all atomic bonds rotate during shear deformation, the angle φ_{ij} is directly related to the local atomic shear strain.

Figs. 2(a)–(c) show the excessive strain distribution of a slice parallel to the xz plane of the Zr–Cu amorphous alloy after 10, 50, and 100 tensile cycles at $\sigma_{max} = 2$ GPa. The 2D sliced plots in Fig. 2 are extracted from our 3D simulation results for the ease of presentation. In these images, the green-color sphere indicates the higher strain levels, while the blue-color sphere indicates small (or zero) strains. During cyclic loading, there are two kinds of deformation mechanism in atomic scale concurrently to dominate the deformation process. One is the elastic deformation with the reversible atomic rearrangement, and the other is the plastic deformation with the irreversible atomic rearrangement. The similar phenomenon is the reduction of the free energy around the deformed areas. From Fig. 2, most of individual excessive strains would accumulate with increasing cycle number. An individual STZ has been suggested to be 15 Å in diameter or so, corresponding to approximately 120 atoms for the CuTi glass model [29]. In our simulation results, these irreversible-deformation atoms constructed the independent STZs distributed in the metallic glass stochastically at the early stages of the current simulation, as shown in Fig. 2(a). At this initial stage, the STZs in Fig. 2(a) with a higher strain level in a green color have a size about 10–20 Å, consistent with the finding of Zink *et al.* [29]. Hence, the irreversible events dominate the majority of the deformation and lead to the development of STZs under cyclic loading. With increasing tensile loading cycles, the larger plastic-strain zone is originated from the connection of each individual STZ, as shown in Fig. 2(b).

However, the distribution of shear strains does not seem to lie along a specific direction, even after finishing 100 loading cycles. This result is different from the case which the linear distribution of shear strains is localized along a specific direction (±40–60°) with respect to the loading axis [30]. The progress of these excessive strains tend to, moreover, connect to form a network-like organization existing in the 3D space semi-homogeneously, such as the green color shown in Fig. 2(b) and (c). The initiation of these STZs and the 3D network strains are similar to the observation of a nanopillar of Zr–Cu–Al glass under compression [19] as well as the cycling-loading simulations of Bulatov and Argon [31]. Apparently, there is no shear localization created in this amorphous matrix, instead, homogeneous shear flows contributed by STZ groups. Although these STZs developed gradually in the matrix, the growth rate of shear deformation appears to become slower in the medium and final stages as compared with that in the early stage, even reaching one hundred cycles, as depicted in Fig. 2(c).

The statistics of accumulating deformations in the stress-control can help understand the growth behavior of flow defects during the cyclic loading. The numbers of deformed atoms, which are in green color in Fig. 2, are gathered in Fig. 3. The deformed atom number rises quickly in the early stage and becomes gradually saturated in later stages. This tendency corresponds well to the observation in the sliced plots in Fig. 2, with apparent difference in STZ numbers between Fig. 2(a) and (b) but minor difference between Fig. 2(b) and (c); the development of STZs seems to be saturated after ~50 cycles. The gradual saturation tendency of the deformed atom numbers or the growth rate of plastic flows, with increasing cycles implies a resistance against the further development of STZ groups once the accumulating deformation reaches a specific level during the cyclic loading.

4. Structural characterization

The structural state of the glassy $Zr_{50}Cu_{50}$ sample after 100 loading cycles is identified by a partial radial distribution function

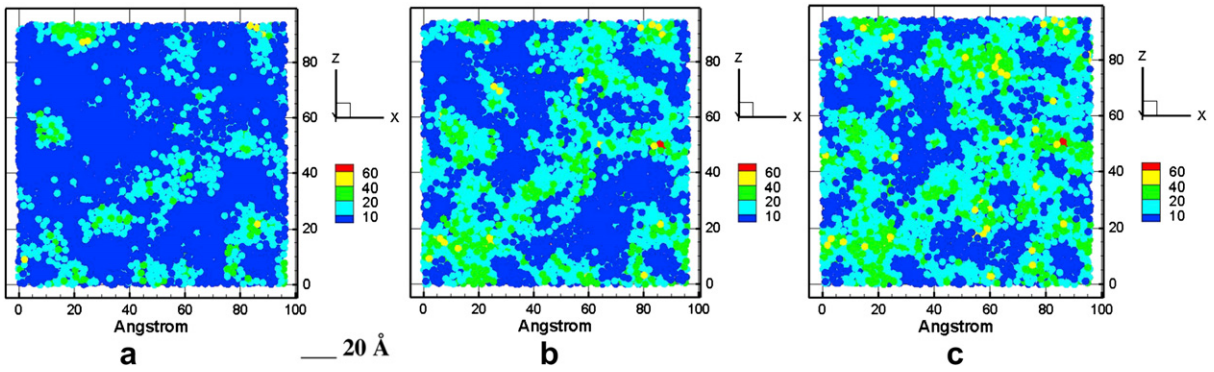

Fig. 2. 2D sliced plots extracting from the 3D simulated results for the local strain distribution of the stress-control fatigue at different cycles: (a) cycle ten, (b) cycle fifty, and (c) cycle one hundred. The color scheme represents the degree of the atomic-bond rotation, or shear strain. The numbers of the horizontal and vertical axes are in the unit of angstrom. (For interpretation of the references to colour in this figure legend, the reader is referred to the web version of this article).

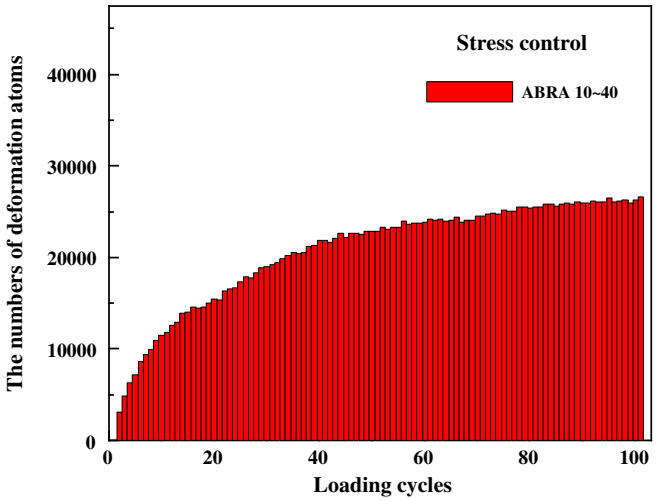

Fig. 3. The accumulation numbers of deformation atoms as a function of loading cycles corresponding to the results of stress-control mode in Fig. 5. The change of growth rate of plastic flows implies a resistance against the sustained development of STZ groups occurs when accumulation deformations reach a specific amount during the cyclic loading. (For interpretation of the references to colour in this figure legend, the reader is referred to the web version of this article).

(PRDF) method which provides the atomic-pair information for the liquid or amorphous structure [24], as shown in Fig. 4(a). The distinctly splitting phenomena occurring for the second peak among the $g_{Cu-Cu}(r)$, $g_{Zr-Zr}(r)$, and $g_{Cu-Zr}(r)$ curves of PRDF are similar to the results of Duan *et al.* [24], in which an amorphous phase was claimed to be produced under a cooling rate of 5 K/ps. After 100 cycles of the tensile loading test, the PRDF curves for the $Zr_{50}Cu_{50}$ specimen in Fig. 4(a) did not show an apparent change during the whole deformation process, still similar to the as-quenched state without crystallization.

Subsequently, a structural analysis proposed by Honeycutt and Anderson [32] is used to study the local symmetry of the atomic arrangement within short-range ordering during the transformation process in the simulation model. This approach provides very clear information about the local symmetry of atomic arrangement more than the radial distribution function, and has been used to study microstructure transition, local cluster structure, and glass forming of metallic alloys under the rapid cooling condition [33,34]. According to this method, different HA indices will represent different local structures. Three pair numbers, namely 1551, 1541, and 1431 pairs, are referred to the common short-range local structures of an amorphous or liquid state, as shown in Fig. 4(b). The trend in Fig. 4(b) means that the local structures with short-range ordering were indeed changed in response to the cyclic loading, but could be relaxed back to the amorphous state upon unloading or reversed loading. This detailed HA-pair analysis shown in Fig. 4(b) explains why there is no major change in the PRDF curves of Fig. 4(a). Although shear deformations are accumulated with increasing cyclic loading, it does not cause permanent structure transitions in the current Zr–Cu amorphous alloy. Instead of no phase transformation in $Zr_{50}Cu_{50}$ metallic glass during cyclic loading in this work, the structural behaviors are always in a periodical fluctuation that indicates the domination of structure properties in its cyclic loading is straightforward structural relaxation. The evidence is the observation of potential energy variation discussed in next section, which always shows a decrease tendency with increasing loading cycles in this work.

5. Viewpoint from energy and density profiles

The variation of the potential energy and alloy density during the course of cycling loading are presented in Fig. 5. Note that the initial energy is −5.233 eV for the as-quenched state. In Fig. 5, the energy increases to −5.231 eV upon the first tensile loading cycle as a result of the stored deformation energy. With continuous cycling loading, the energy gradually relaxes to −5.235 eV at the end upon unloading (only 0.04% decrement as compared with the as-quenched state). The density shows a minor change from the as-quenched state (7.29 g/cm^3) to 7.295 g/cm^3 at the end upon unloading (just about 0.07% increment), suggesting a slight decrease in free volumes via variation of energy during cyclic loading.

Dynamic recovery induced by cyclic loading appears to have occurred in this stress-control modes, especially significant in the early stages. From the above results, it appears that the whole structures would be relaxed toward a more steady state with a slightly lower potential energy and a slightly higher density state. Compared with Fig. 4(b), it appears that the accumulation of deformation would be accompanied by the relaxation of the local arrangement and minor annihilation of excessive free volumes in the total environment. The variations of the energy and density are more pronounced in the initial few cycles. After reaching a semi-steady state, the energy and density become gradually saturated under loading and unloading states. But deformation could keep on accumulating in the system. This balance between the creation of

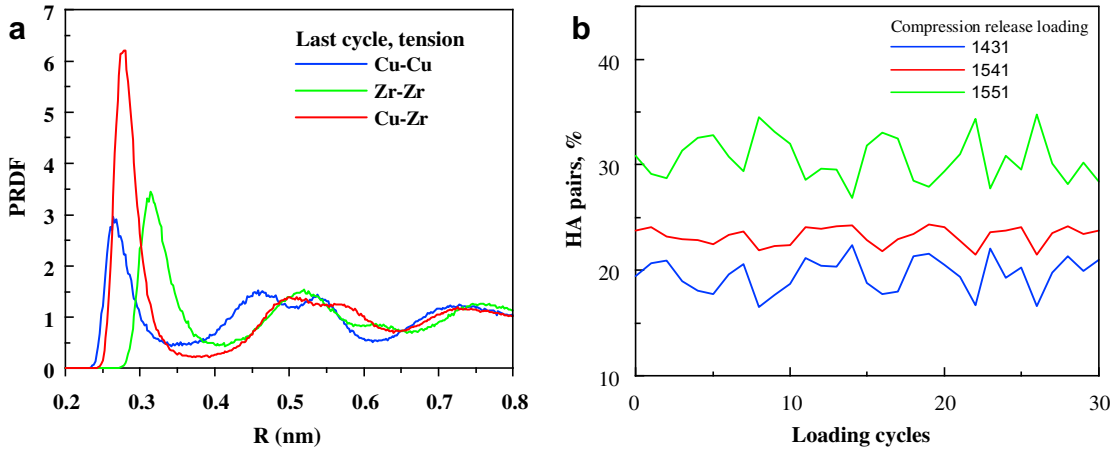

Fig. 4. (a) The curves of different bond pairs of PRDF for the $Zr_{50}Cu_{50}$ amorphous alloy at 300 K after 100 cycles at $\sigma_{max} = 2$ GPa under the stress-control mode. (b) Variations of 1431, 1541, and 1551 HA indices of the Zr–Cu amorphous alloy as a function of loading cycles under cyclic stress-control mode. (For interpretation of the references to colour in this figure legend, the reader is referred to the web version of this article).

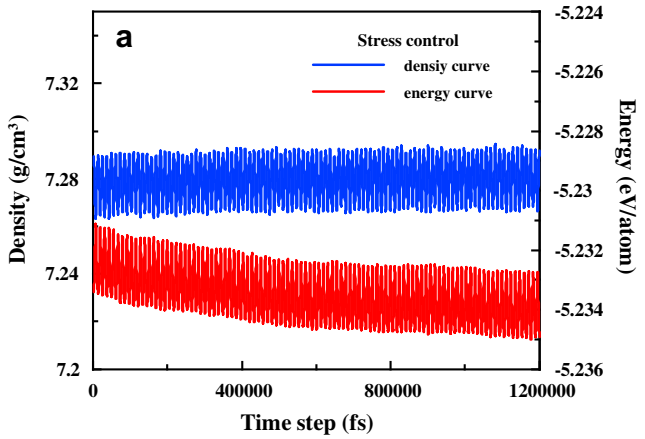

Fig. 5. Variations of the density and energy as a function of the loading-time step at stress-control mode at $\sigma_{max} = 2$ GPa. The blue solid line presents the total density variation and the red dotted line presents the variation of the average potential energy per atom. (For interpretation of the references to colour in this figure legend, the reader is referred to the web version of this article).

free volume by STZ and the annihilation by relaxation processes are corresponding to the phenomenon of homogeneous flow in a steady state typically. Structural relaxation usually plays an important role that would lead the metallic glass to transfer to lower energy states in the potential energy landscape through the atomic motion when annealing at a high enough temperature, but insufficient for crystallization [9]. The simulation results of HA analysis and potential energy variation apparently prove that cyclic loading in the homogeneous deformation of metallic glass can provide enough atomic kinetics to leap over the energy barrier for next metastable equilibrium driven by mechanical-induced relaxation processes. Through the cyclic structural relaxations, the local strain could accumulate in the current system, resulting in the development of shear flows gradually.

6. The phenomenon of dynamic recovery and structural relaxation

In the crystalline materials, dynamic recovery proceeds mainly via the rearrangement of dislocations cell walls or subgrain boundaries. And dynamic recovery occurs more easily in metals with high stacking-fault energy. In amorphous structures, local atoms suffered shear deformation could result in stacking-fault-like energy [15,35], and the derivative of this stacking-fault energy could become the resistance traction to hold back the highly localized shearing in the metallic glass. This event could cause the local instability of the deformed atomic clusters, and thereby dynamic recovery could be induced to occur via the mutual activation of STZ groups that are discretely generated by the cyclic deformation as the results in Fig. 2. This behavior is similar to the model of reversible/irreversible structural relaxation of metallic glasses [36–39], but it is nearly diffusionless, different from the thermal recovery caused by structural relaxation in high-temperature annealing or creep. The cyclic deformation at room temperature can also provide mechanical-energy input for the relaxation reaction.

The self-repairing structural relaxation and dynamic recovery of metallic glasses under cyclic loading is proposed below. When an amorphous structure is achieved by quenching, it may be composed of icosahedral local short-range ordering, network-forming clusters medium-range ordering, and other unidentified-random local structures [36,40]. With the complex atomic packing, some places are more easy to undergo structural relaxation (i.e., with a higher degree of loose bonds or free volumes), termed as the relaxation centers (RCs) in the metallic glasses [37,38]. Some of them are regarded as the reversible relaxation centers (RRCs) and others irreversible relaxation centers (IRRCs). The distribution and organization of such relaxation centers are believed to be sensitive to cooling rate. The RRCs are inherent with a more symmetrical potential barrier state in space, as depicted in Fig. 6(a). When the local atoms around RRCs are subjected to local shear stress, atoms are separated from their original positions into a new atomic arrangement. The energy states of the original and new atomic arrangements are both at the similar semi-stable level, and parts of new atomic arrangements belonging to RRCs tend to recover back to their original atomic arrangement state upon the applied stress is relieved or during reversed loading. Such atomic arrangement back and forth is reversible, and occurs predominantly when the applied loading stress/strain is small and within the elastic or early plastic regime (to around 2–2.5% strain). The fatigue-loaded Zr–Cu metallic glass, though subjected to long-cycle fatigue, still behaves undamaged, as if there have been local self-repairing dynamic recovering mechanisms during cyclic deformation.

On the other hand, the IRRCs are inherent with an asymmetrical potential barrier state, as shown in Fig. 6(b). Parts of atoms belonging to IRRCs, under shear stress, would like to jump into a more compatible and stable state (with a lower energy) while the other atoms go to fill a vacant free volume. The occurrence of such irreversible plastic events would lead STZs to keep on accumulating and growing gradually inside the amorphous material. Such local plastic events during structural relaxation/recovery would benefit the annihilation or removal of defects (e.g. free volume) by moving the system toward a more stable state at each cycle. Such a new atomic arrangement possesses a tighter bonding. Since the new atomic arrangement is in the lower energy state, it is unlikely to return back to the original arrangement, behaving as irreversible relaxation. This behavior can be viewed as a self-repairing dynamic recovery process that the defects induced in the previous cycle could be eliminated in the subsequent cycle. This self-repairing dynamic recovery phenomenon during cyclic loading also results in the temporary appearance and disappearance of local STZs, reducing the tendency for massive STZ pile-up to form a damaging macro shear band.

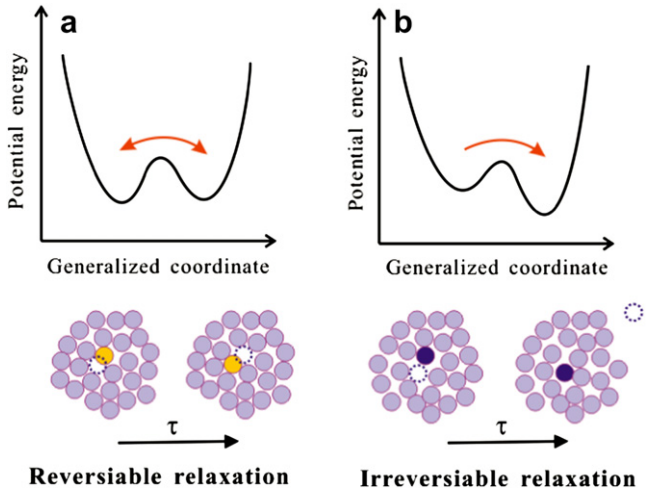

Fig. 6. The schematic drawings of metallic glass showing the models of dynamics recovery during cyclic loading: (a) the dynamic recovery model of reversible relaxation centers (RRCs) with a symmetry potential barrier which causes the local elastic events during the cyclic loading process, (b) the dynamic recovery model of irreversible relaxation centers (IRRCs) with an asymmetry potential barrier which causes the local plastic events during the cyclic loading process. (For interpretation of the references to colour in this figure legend, the reader is referred to the web version of this article).

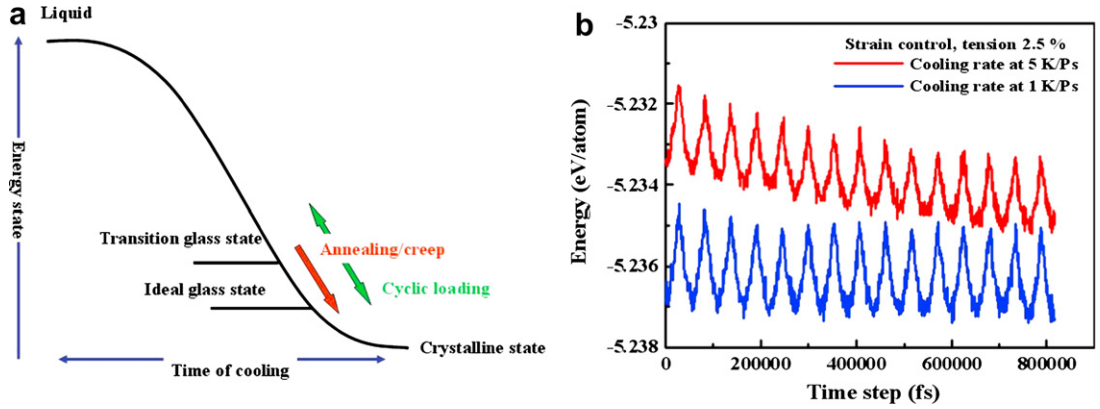

Fig. 7. (a) Schematic illustration of the effect of stress-induced relaxation on its energy landscape, and (b) the comparison of potential energies between two amorphous samples as-quenched at different cooling rates suffered the same strain rate during cyclic loading. The results show that mechanical-induced relaxation can cause a dynamic recovery on its energy state to approach the lower one which can be reached through slow cooling rate or creep. (For interpretation of the references to colour in this figure legend, the reader is referred to the web version of this article).

Actually, it is very difficult to get an ideal amorphous which is in the lowest energy state from rapid cooling. It is mostly easy to be in a transition glass state depending on time of cooling, as shown in Fig. 7(a). Hence, structural relaxation plays an important role that can lead the metallic glass to transfer to lower energy states in the potential energy landscape through the atomic motion when annealing at a high enough temperature, but insufficient for crystallization [9]. Although a true phase in the metallic glass is still unclear so far, it can be speculated from this work that cyclic loading in homogeneous deformation can stimulate transition glass state from as-quench to leap over the local energy barrier continuously. In theoretical, one can approach gradually to an ideal glass by this way, as illustrated in Fig. 7(a). This inference has been proved in Fig. 7(b), which shows this simulation result of strain control applied on two models at different as-quenched states.

The current simulation results suggest that the metallic glass in small size-scale can be quite fatigue resistant. The metallic bonds in the metallic glasses, once broken by local shear stress, can be self-repaired and re-bonded to neighboring atoms by the subsequent reverse shear stress. Such a dynamic recovery capability is particularly significant in cyclic loading of homogeneous flow. For applications of the metallic glasses in micro-electro-mechanical systems (MEMS) [41], the current finding is encouraging.

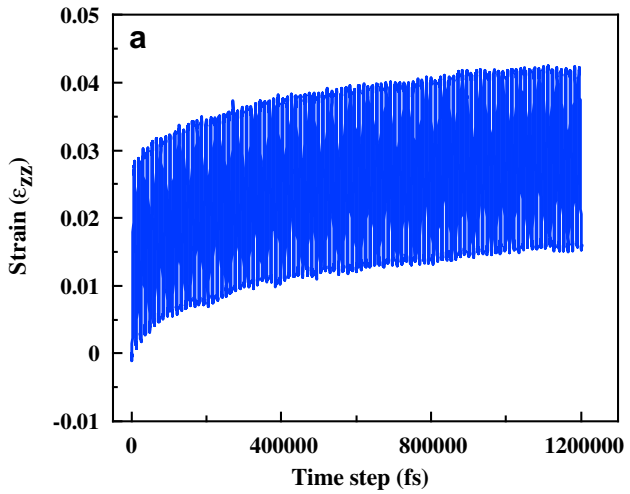

Fig. 8. Variation of (a) the induced strain as a function of the fatigue cycle for the stress-control mode at $\sigma_{max} = 2$ GPa. (For interpretation of the references to colour in this figure legend, the reader is referred to the web version of this article).

7. Softening or hardening in cyclic loading?

It is of interest to examine whether the cyclically-loaded specimen in this work would exhibit softening, hardening, or constant strength during the course of cyclic loading. Crystalline materials have shown all these three kinds of behaviors, depending on the materials nature and the loading conditions. The current Zr–Cu metallic glass is found to show a slight cyclic-softening behavior, particularly for the initial stage upon the first cycle, as shown in Fig. 8. As shown in Fig. 8, the induced strain gradually increase from the 2.8% strain upon the first tension cycle, then to a 3.6% strain after 25 cycle, to a 3.9% strain after 50 cycles, and finally to a 4.1% strain after 100 cycles. It appears that the amorphous Zr–Cu alloy was soon softened upon the initial cycling stage and gradually reaches a semi-saturated state.

For the more severe tension-compression strain-control test (not shown in this paper), the measured stress decreases appreciably from 3.0 GPa for the first cycle, to 2.5 GPa for the second cycle, and fluctuates within 2.5–2.7 GPa during the subsequent cycles. It seems that the severe first-cycle loading has induced a certain amount of defects or free volumes in this case, causing the initial softening. The following cycling loading does not render further softening after first-cycle loading. The induced defects or free volumes would be dynamically recovered, lessening the cyclic-loading softening. Overall, the current Zr–Cu metallic glass, in small size-scale, appears to exhibit only minor softening behavior.

8. Conclusion

Through the molecular dynamics studies of the cyclic loading response of $Zr_{50}Cu_{50}$ metallic glasses under the stress-control mode at $\sigma_{max} = 2$ GPa, the following conclusions can be reached.

(1) The current simulated results demonstrate that the induced STZs, measuring 10–20 Å, are basically discrete and homogeneous. The temporary local STZs formed in one loading cycle frequently disappear in the subsequent unloading or reversed-stress loading cycles.
(2) Based on the deformation evolution as a function of cyclic loading, evident by the simulated ABRA, potential energy, atomic density, and strain softening results, the current Zr–Cu amorphous alloy appears be deformed more readily in the initial fatigue stage, followed by gradual saturated behavior due to the balance between the creation/annihilation of excessive free volume in homogeneous flow.

(3) Throughout the current cyclic deformation under the stress-control mode, there are no major atomic structure changes or stress-induced crystallization, as judged from the PRDF and HA index. This is thought to be a result of the limited simulated volume, within which the STZs are still in their early development. The mature shear bands are not yet fully developed.
(4) It is found that structure relaxation, or dynamic recovery, has occurred in the current cyclic loading of the Zr–Cu metallic glass. When the loading stress is low, still well within the elastic or early plastic range, the dynamic recovery of RRCs will dominate the most atomic events. When the loading stress or strain exceeds into the plastic regime, dynamic recovery of IRRCs becomes easier.
(5) Through the self-repairing and dynamic recovery capability of IRRCs, the current Zr–Cu metallic glass could reduce the local spatial defects in STZs induced by the previous cyclic deformation. Thus the overall metallic glassy structure under cyclic loading could resist the damage accumulation, exhibiting satisfactory fatigue resistance.
(6) The current simulation results suggest that the metallic glass in small size-scale can be quite fatigue resistant. The metallic bonds in the metallic glasses, once broken by local shear stress, can be self-repaired and re-bonded to neighboring atoms by the subsequent reverse shear stress. Such a dynamic recovery capability is particularly significant in cyclic loading. For applications of the metallic glasses in micro-electro-mechanical systems (MEMS), the current finding is encouraging.

Acknowledgments

The authors gratefully acknowledge the sponsorship from the National Science Council of Taiwan, ROC, under the project no. NSC 96-2218-E-110-001. YCL would like to thank Prof. S.P. Ju for the use of PC clusters on this calculation works, and Prof. J. Li for useful discussions on the analysis in this paper. PKL is very grateful for the support of the National Science Foundation International Materials Institutes (IMI) Program (DMR-0231320) with Dr. C. Huber as the Program Director. JRM's research has been sponsored by the Division of Materials Sciences and Engineering, Office of Basic Energy Sciences, U.S. Department of Energy under contract with DE-AC05-00OR-22725 with the UT-Battelle.

References

[1] Johnson WL. MRS Bulletin 1999;24:42.
[2] Inoue A. Acta Materialia 2000;48:279.
[3] Wang WH, Dong C, Shek CH. Materials Science and Engineering R Reports 2004;44:45.
[4] Spaepen F. Acta Metallurgica 1977;25:407.
[5] Argon AS. Acta Metallurgica 1979;27:47.
[6] Steif PS, Spaepen F, Hutchinson JW. Acta Metallurgica 1982;30:447.
[7] Wright WJ, Hufnagel TC, Nix WD. Journal of Applied Physics 2003;93:1432.
[8] Kanungo BP, Glade SC, Asoka-Kumar P, Flores KM. Intermetallics 2004;12:1073.
[9] Schuh CA, Hufnagel TC, Ramamurty U. Acta Materialia 2007;55:4067.
[10] Albano F, Falk ML. Journal of Chemical Physics 2005;122:154508.
[11] Li QK, Li M. Applied Physics Letters 2006;88:241903.
[12] Li QK, Li M. Physical Review B 2007;75:094101.
[13] Wang GY, Liaw PK, Peter WH, Yang B, Yokoyama Y, Benson ML, et al. Intermetallics 2004;12:885.
[14] Wang GY, Liaw PK, Peter WH, Yang B, Freels M, Yokoyama Y, et al. Intermetallics 2004;12:1219.
[15] Shimizu F, Ogata S, Li J. Acta Materialia 2006;54:4293.
[16] Li QK, Li M. Applied Physics Letters 2007;91:231905.
[17] Donohue A, Spaepen F, Hoagland RG, Misra A. Applied Physics Letters 2007;91:241905.
[18] Guo H, Yan PF, Wang YB, Tan J, Zhang ZF, Sui ML, et al. Nature Materials 2007;6:735.
[19] Shan ZW, Li J, Cheng YQ, Minor AM, Asif SAS, Warren OL, et al. Physical Review B 2008;77:155419.
[20] Park KW, Lee CM, Lee MR, Fleury E, Falk ML, Lee JC. Applied Physics Letters 2009;94:3.
[21] Park KW, Lee CM, Fleury E, Lee JC. Scripta Materialia 2009;61:363.
[22] Xia L, Fang SS, Wang Q, Dong YD, Liu CT. Applied Physics Letters 2006;88:171905.
[23] Cleri F, Rosato V. Physical Review B 1993;48:22.
[24] Duan G, Xu DH, Zhang Q, Zhang GY, Cagin T, Johnson WL, et al. Physical Review B 2005;71:224208.
[25] Mundy CJ, Balasubramanian S, Bagchi K, Tuckerman ME, Martyna GJ, Klein ML. Reviews in Computational Chemistry 2000;14:291.
[26] Tuckerman ME, Martyna GJ. Journal of Physical Chemistry B 2000;104:159.
[27] Lai YH, Lee CJ, Cheng YT, Chou HS, Chen HM, Du XH, et al. Scripta Materialia 2008;58:890.
[28] Lee CJ, Huang JC, Nieh TG. Applied Physics Letters 2007;91:161913.
[29] Zink M, Samwer K, Johnson WL, Mayr SG. Physical Review B 2006;73:172203.
[30] Shi YF, Falk ML. Physical Review B 2006;73:214201.
[31] Bulatov VV, Argon AS. Modelling and Simulation in Materials Science and Engineering 1994;2:203.
[32] Honeycutt JD, Andersen HC. Journal of Physical Chemistry 1987;91:4950.
[33] Yamakov V, Wolf D, Phillpot SR, Mukherjee AK, Gleiter H. Nature Materials 2002;1:45.
[34] Liu J, Zhao JZ, Hu ZQ. Materials Science and Engineering A Structural Materials Properties Microstructure and Processing 2007;452:103.
[35] Shimizu F, Ogata S, Li J. Materials Transactions 2007;48:2923.
[36] Tanaka H. Journal of Non-crystalline Solids 2005;351:3396.
[37] Khonik VA, Kosilov AT, Mikhailov VA, Sviridov VV. Acta Materialia 1998;46:3399.
[38] Belyavsky VI, Csach K, Khonik VA, Mikhailov VA, Ocelik V. Journal of Non-crystalline Solids 1998;241:105.
[39] Golovin YI, Ivolgin VI, Khonik VA, Kitagawa K, Tyurin AI. Scripta Materialia 2001;45:947.
[40] Sheng HW, Luo WK, Alamgir FM, Bai JM, Ma E. Nature 2006;439:419.
[41] Kumar G, Tang HX, Schroers J. Nature 2009;457:868.